



## OPEN ACCESS

## EDITED BY

Lingling Zhao,  
University of Alabama in Huntsville,  
United States

## REVIEWED BY

Krishna Khanal,  
The University of Alabama in Huntsville,  
United States  
Xingyu Zhu,  
The University of Alabama in Huntsville,  
United States

## \*CORRESPONDENCE

Xiaocheng Guo,  
✉ [xcguo@swl.ac.cn](mailto:xcguo@swl.ac.cn)

RECEIVED 04 December 2025

REVISED 14 January 2026

ACCEPTED 19 January 2026

PUBLISHED 09 February 2026

## CITATION

Yue J, Guo X, Wang Y and Wang C (2026)  
Contribution of magnetotail currents to Dst  
index during different intensity magnetic  
storms: a global MHD model study.  
*Front. Astron. Space Sci.* 13:1760941.  
doi: 10.3389/fspas.2026.1760941

## COPYRIGHT

© 2026 Yue, Guo, Wang and Wang. This is an  
open-access article distributed under the  
terms of the [Creative Commons Attribution  
License \(CC BY\)](https://creativecommons.org/licenses/by/4.0/). The use, distribution or  
reproduction in other forums is permitted,  
provided the original author(s) and the  
copyright owner(s) are credited and that the  
original publication in this journal is cited, in  
accordance with accepted academic practice.  
No use, distribution or reproduction is  
permitted which does not comply with  
these terms.

# Contribution of magnetotail currents to Dst index during different intensity magnetic storms: a global MHD model study

Jiawen Yue<sup>1,2</sup>, Xiaocheng Guo<sup>1,2\*</sup>, Yuxian Wang<sup>1</sup> and Chi Wang<sup>1,2</sup>

<sup>1</sup>Key Laboratory of Solar Activity and Space Weather, National Space Science Center, Chinese Academy of Sciences, Beijing, China, <sup>2</sup>College of Earth and Planetary Sciences, University of Chinese Academy of Sciences, Chinese Academy of Sciences, Beijing, China

The Disturbance Storm Time (Dst) index serves as a critical indicator for quantifying geomagnetic storm intensity; however, the precise contribution of magnetotail currents to its formation remains inadequately characterized. Based on a global magnetospheric magnetohydrodynamics (MHD) model, this study quantifies the contribution of magnetotail currents to the Dst index during geomagnetic storms of varying intensities. The Biot-Savart law was applied to integrate the magnetotail current density, computing the corresponding magnetic perturbation at Earth center in order to quantify the contribution of the magnetotail current to the Dst index. This study analyzed 20 geomagnetic storm events spanning varying intensities, with the majority occurring within the past 5 years. Simulation results indicate that the quantified contribution of magnetotail currents ranges from 23% to 26% during moderate storms, 20%–24% during intense storms, and falls below 20% during super storms. Thus, the relative contribution of magnetotail currents exhibits a robust decreasing trend with increasing storm intensity. This study is the first to employ a global MHD model to systematically quantify the contribution of magnetotail currents to the Dst index across varying geomagnetic storm intensities. These findings provide crucial quantitative evidence for understanding the role and dynamics of the magnetotail current system in geomagnetic storms, particularly highlighting its diminishing relative contribution during severe space weather events.

## KEYWORDS

Dst index, magnetic storm, magnetosphere, magnetotail current, MHD, simulation

## 1 Introduction

The magnetotail is a crucial component of Earth's magnetosphere, located on the planet's nightside. It serves as a dynamic reservoir where solar wind energy is stored and subsequently released to trigger phenomena such as substorms (Rostoker et al., 1988; Nishida, 2000; Nakamura, 2007). Based on distance from Earth, the magnetotail is conventionally divided into two regions: the near-Earth magnetotail (adjacent to the planet) and the distant magnetotail, extending outward to several hundred Earth radii. Key plasma regimes within the magnetotail include the plasma sheet and its boundary layer, the magnetotail lobes,

the magnetopause boundary layer, and the distant magnetotail (Bame et al., 1967; Frank, 1985). The spatial scale and current density of the Earth's magnetotail current sheet determine its configuration, which is critical to substorms—the most energetically powerful phenomena in the Earth's magnetosphere (Liu et al., 2013; Artemyev et al., 2021). Magnetic reconnection is a fundamental process in space plasmas, characterized by the breaking and reconnection of magnetic field lines. This process rapidly converts magnetic energy into the kinetic and thermal energy of particles, resulting in explosive energy release (Torbert et al., 2018; Hesse and Cassak, 2020; Ji et al., 2022). It not only drives auroral phenomena but also underpins space weather events such as geomagnetic storms.

The magnetotail current system is a crucial component of Earth's magnetosphere, forming in the magnetotail region on the nightside and playing a significant role in magnetospheric dynamics. These currents are primarily generated by charged particles—mainly electrons and protons—that originate from the solar wind, become energized, and subsequently travel along the geomagnetic field lines into the magnetotail (Bird, 1974; Artemyev and Zelenyi, 2013). Within the magnetotail, two main types of currents are present: field-aligned currents, which flow along the magnetic field lines and couple the magnetotail with Earth's upper atmosphere, playing an essential role in the formation of auroras (Frank et al., 1981; Kamide, 1982); and the cross-tail current sheet, often referred to as the plasma sheet current, which forms a closed loop within the central magnetotail. These currents are central to the storage and explosive release of energy in the magnetosphere, driving phenomena such as substorms, auroras, and geomagnetic storms (Rostoker, 1996; Runov et al., 2021). Understanding their structure and dynamics is essential for both space weather prediction and fundamental plasma physics.

The Dst index is a widely used measure of geomagnetic activity (Sugiura, 1960), specifically designed to quantify the intensity of the Earth's magnetospheric ring current during geomagnetic storms. The Dst index has a temporal resolution of 1 h, which may not be sufficient to capture rapid geomagnetic fluctuations. To overcome this limitation, the SYM-H index was introduced as an alternative with a higher temporal resolution of 1 min (Iyemori, 1990). Unlike the Dst index, which is calculated by removing the average quiet-time variation from the horizontal magnetic field components recorded at four low-latitude geomagnetic stations that are approximately evenly distributed worldwide, SYM-H is calculated using data from six ground magnetometer stations spanning from low to mid-latitudes with stations evenly distributed in longitude along the equatorial region (Wanliss and Showalter, 2006). This improved spatial coverage allows SYM-H to provide a more comprehensive representation of the ring current's global behavior during geomagnetic disturbances.

While the Dst index is primarily interpreted as a proxy for the ring current, it also reflects contributions from other magnetospheric current systems. Notably, the magnetotail current system contributes to Dst fluctuations during geomagnetic storms. However, the relative impact of the magnetotail current on the Dst index remains a subject of debate in the literature. Turner et al. (2000) employed the T96 and T89 models to calculate the influence of magnetotail region currents on ground magnetic field measurements (and consequently the

Dst index), revealing that for geomagnetic storms with Dst approximately  $-80$  nT the magnetotail current contribution to Dst ranges from  $-22$  to  $-26$  nT and demonstrating an approximate linear relationship between Dst index and magnetotail current contribution which accounts for approximately one-quarter of total Dst values. Ohtani et al. (2001) estimated, by correlating the timing of geosynchronous dipolarization with the Dst (SYM-H) minimum, that the tail current contributes approximately 20%–25% to the index at its minimum value.

Tsyganenko (2002) demonstrated through empirical modeling of the Earth's inner and near magnetosphere that the innermost portion of the tail cross-sectional current exhibits high sensitivity to southward IMF and accounts for approximately 90% of the tail's influence on the Dst index, whereas more distant tail currents primarily respond to solar wind dynamic pressure with negligible contribution to the Dst index. Skoug et al. (2003) investigated a superstorm using combined spaceborne and ground-based observations. By analyzing the highly localized nightside distribution of energetic neutral atoms (ENAs) and ground magnetometer disturbances, they demonstrated that the tail current, rather than the ring current, was the dominant contributor to the Dst index during the storm's main phase. Ganushkina et al. (2004) modeled three moderate geomagnetic storms and one intense geomagnetic storm, revealing that the ring current dominates during intense storms whereas the near-Earth magnetotail current contributes more to the Dst index than the ring current during moderate storms.

Kalegaev et al. (2005) employed three distinct magnetospheric magnetic field models to simulate two geomagnetic storm events and quantified the contributions of ring current, tail current, and magnetopause current to the Dst index, revealing that during moderate-intensity storms the tail current contributes significantly to the Dst index comparably to the ring current, while during intense storms the ring current becomes the dominant source. Kalegaev and Makarenkov (2008) conducted a statistical investigation of 70 magnetic storms with varying intensities using the paraboloid magnetospheric model A2000, revealing that the ring current becomes the dominant contributor to Dst during intense magnetic storms while its contribution matches that of the tail current during moderate storms, with the ring current injection amplitude increasing as magnetospheric disturbance levels intensify and the tail current effect approaching saturation under extreme disturbance conditions. Ganushkina et al. (2010) employed two different modeling approaches: the event-oriented empirical magnetic field model and the SWMF model based on global MHD simulations demonstrating that in moderate geomagnetic storms the event-oriented model revealed wake current dominance during the event while the SWMF results showed no significant wake current development during the main phase. Asikainen et al. (2010) proposed a semi-empirical model utilizing the isotropic boundary (IB) position of high-energy particles observed by NOAA/POES satellites as a proxy for tail current intensity, concluding that the tail current's average contribution to the Dcx index (a more correct version of the Dst index) accounts for approximately 34%.

Patra et al. (2011) investigated multiple geomagnetic storm events during 2000–2007 using the WINDMI model of the nightside magnetosphere demonstrating that under IMF Bz northward conditions the magnetotail current contributes significantly to

the rapid initial decay of the Dst index in the early recovery phase of magnetic storms while the later slower recovery phase Dst decay is predominantly determined by ring current decay driven by charge exchange processes. Ganushkina et al. (2012) employed two different modeling approaches (magnetic field modeling and particle modeling) to simulate the configuration of inner magnetospheric current systems, namely the ring current and near-Earth tail current, during magnetic storm events, both approaches demonstrating that incorporating the near-Earth tail current is crucial when computing the modeled Dst index (referred to as SYM-H in the study) since the simulation results show significant currents beyond  $6.6 R_E$  ( $R_E$  is Earth's radius). Kalegaev and Ganushkina (2013) employed two magnetic field models to investigate moderate and intense magnetic storms revealing that the ring current's contribution to Dst is comparable to the tail current during moderate storms but dominates during intense storms. Pulkkinen et al. (2022) presents geomagnetic storm simulations showing that magnetotail and ring currents correlate closely with Dst index, revealing a significant tail current contribution beyond  $8 R_E$  to Dst during storm main phase.

While previous quantitative studies on the linkage between magnetotail currents and the Dst index have largely relied on empirical models and statistical methods, investigations employing physics-based global magnetospheric MHD models remain scarce. This study investigates the contribution of magnetotail currents to the Dst index through numerical simulations using a global magnetospheric MHD model. The paper is structured as follows: Section 2 presents the simulation performance of the global MHD model in reproducing magnetotail currents and describes the methodology for calculating the contribution of these currents to the Dst index; Section 3 details the selected geomagnetic storm events and datasets, as well as the model performance evaluation metrics employed in the analysis; Section 4 presents the simulation results and analyzes the relative contributions of magnetotail currents to the Dst index across storm events of varying intensities; Section 5 provides a comprehensive discussion, encompassing an analysis of extreme values, the temporal evolution and uncertainty of the contributions, their sensitivity to the definition of the magnetotail region, and a synthesis of the storm-intensity-dependent trend; finally, Section 6 provides a comprehensive summary and concludes the study.

## 2 Computing the Dst contribution from simulated magnetotail currents

As noted in the previous section, the Dst index is commonly used to quantify the overall intensity of geomagnetic activity at low latitudes and serves as a proxy for estimating the energy density of the ring current near Earth. In addition to the ring current, other magnetospheric current systems, such as the dayside magnetopause currents and the nightside magnetotail currents, also cause ground magnetic disturbances and contribute to the Dst index to some extent (Temerin and Li, 2006). To simulate the magnetospheric currents, we use an extended version of the PPMLR-MHD model (Hu et al., 2007). The simulation employs a three-dimensional stretched grid in GSM coordinates, with the highest resolution of  $0.4 R_E$  in the near-Earth region, extending

to cover the domain from  $-120 R_E$  to  $30 R_E$  in X and  $\pm 70 R_E$  in Y and Z directions. This version incorporates an HLL-type Riemann solver, extended specifically for intrinsic magnetic field decomposition. Within the MUSCL numerical scheme, this solver is applied to update the numerical fluxes at computational cell interfaces (Guo, 2015; Guo et al., 2016). During each simulation time step, the magnetic field  $\mathbf{B}$  at all grid nodes across the global domain is synchronously updated by solving the full set of MHD governing equations. The magnetospheric current system originates from the global distortion of the Earth's magnetic field under sustained solar wind forcing, enabling direct derivation of the current density distribution through the normalized Ampère's law,  $\mathbf{j} = \nabla \times \mathbf{B}$ . This approach effectively characterizes large-scale magnetospheric structures including the magnetopause currents, field-aligned currents, and magnetotail neutral sheet currents. It should be noted that the standard single-fluid MHD model employed here has inherent limitations in describing inner magnetospheric dynamics: the model does not incorporate physical mechanisms accounting for charged particle gradient drift and curvature drift effects, thereby precluding self-consistent simulations of ring current formation and evolution processes.

Figure 1 presents the simulated magnetospheric current density distributions from the global magnetospheric MHD model for the 15th storm event listed in Table 1 (next chapter). The distributions are shown at two distinct time points: during the quiet period before the storm sudden commencement and at the moment when the Dst index reaches its minimum value. To circumvent the significant errors in current calculation induced by the extremely strong magnetic field gradient near Earth and to avoid an impractically small evolution time step due to the extremely high local Alfvén speed, the MHD model implements an inner boundary in the near-Earth region. In global magnetospheric simulations, the inner boundary is typically set between  $2.5$  and  $3.5 R_E$  to balance physical realism with numerical stability (Ridley et al., 2010; Rastätter et al., 2013; Chen et al., 2017). For this study, a value of  $3 R_E$  was adopted. As observed in Figure 1a, the current density distribution during the quiet period is distinctly visible, with clear identification of the bow shock current, magnetopause current, and magnetotail current. As previously indicated in the text, due to inherent limitations of the MHD model, the ring current cannot be adequately resolved. During this relatively quiescent period, the magnetosphere exhibits a stable configuration. In the X-Z plane view, the current magnitudes in the magnetotail region are weaker than those at the dayside magnetopause but still stronger than the nightside currents. In contrast, Figure 1b demonstrates significant changes at the storm's main phase when the Dst index reaches its minimum. While distinct current structures remain identifiable across all regions, their magnitudes show substantial increases compared to the quiet period. The magnetopause region exhibits clear compressional features, with the subsolar bow shock shifting inward from  $\sim 15.3 R_E$  to  $\sim 9.7 R_E$  (a displacement of  $\sim 5.6 R_E$ ) as seen in the X-Z plane. The magnetotail current occupies a notably expanded spatial extent with significantly enhanced current densities relative to the quiet-time conditions, as revealed in the X-Z plane distribution.

In this study, the estimation of the Dst index does not rely on local observations from specific geomagnetic observatories, but instead is based on the spatially averaged characteristics of magnetic

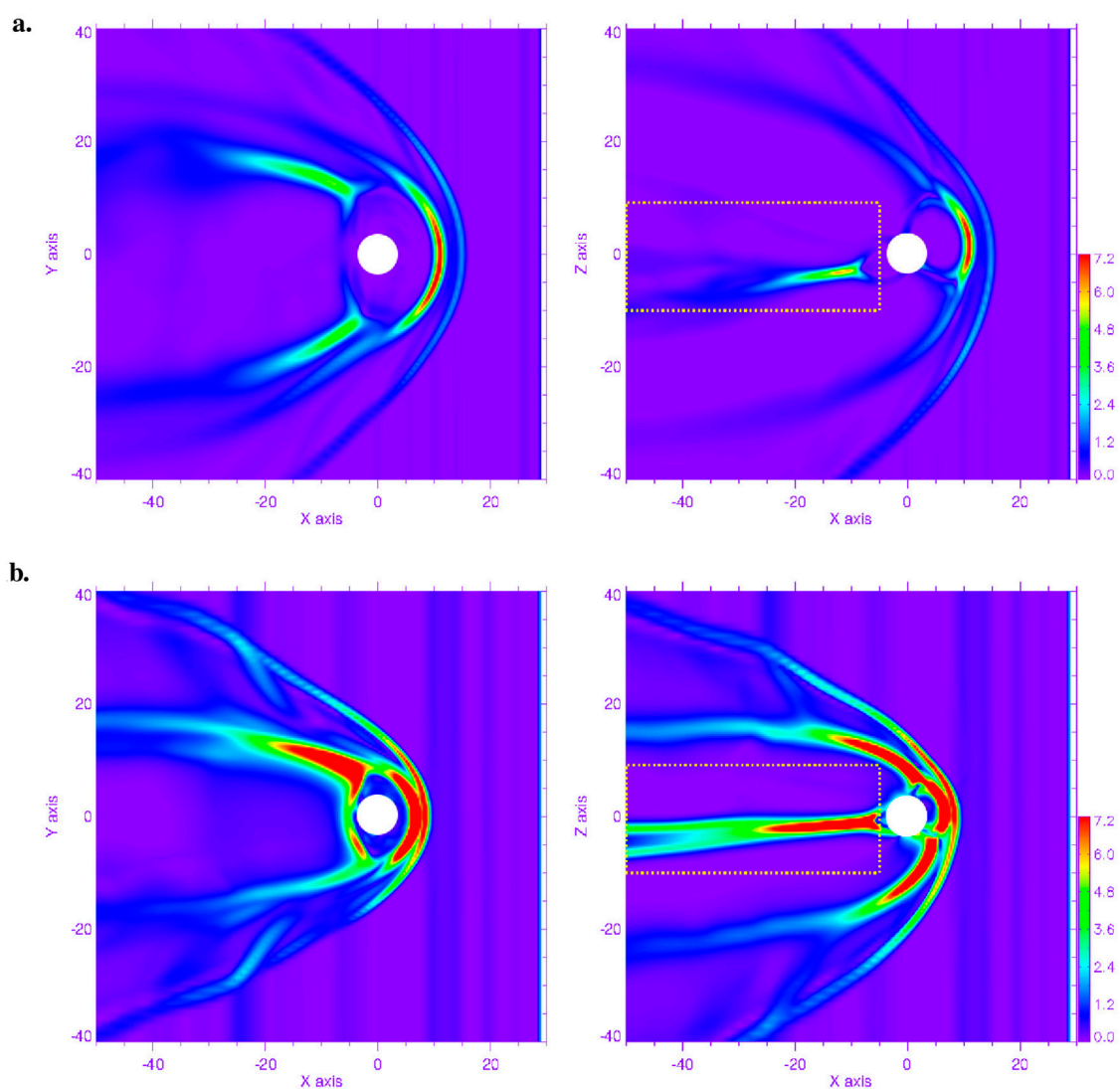


**FIGURE 1** Figure showing the magnetospheric current density distributions simulated by the global magnetospheric MHD model for the 15th intense geomagnetic storm event listed in Table 1. The GSM coordinate system is adopted, depicting the (left) X-Y plane and (right) X-Z plane. The magnetotail region selected in this study is enclosed by a yellow rectangular box. Current density units are in nA/m<sup>2</sup>, with color-to-value correspondence detailed in the colorbar on the right. **(a)** Quiet period prior to the storm sudden commencement. **(b)** During the storm main phase when the Dst index reached its minimum value of -136 nT. **(a)** Simulated magnetospheric current density distribution in the GSM coordinate system at 00:10 UT on 1 December 2023 (quiet period) using the global magnetospheric MHD model, with units in nA/m<sup>2</sup>. **(b)** Simulated magnetospheric current density distribution in the GSM coordinate system at 13:30 UT on 1 December 2023 (Dst = -136 nT) using the global magnetospheric MHD model, with units in nA/m<sup>2</sup>.

field disturbances at the Earth center, reflecting the overall level of geomagnetic disturbances in the equatorial region. Following the modeling strategies widely adopted in global MHD simulations, the Dst index is defined as the north-south component of the disturbance field in geocentric coordinates. This approach is widely adopted in global MHD simulations as a physically consistent proxy for the ground-based Dst index (Rastätter et al., 2013; Liemohn et al., 2018). The rationale is that the large-scale magnetospheric current systems, such as the magnetopause, tail, and ring currents, are the primary sources of low-latitude magnetic disturbances. The perturbation field at Earth center  $\delta B_z$  calculated from these currents via the Biot-Savart law captures the essence of their combined effect, which is what the Dst index ultimately

measures. While this proxy may differ from the observed Dst in absolute baseline and detailed amplitude due to the omission of induction effects, crustal fields, and the specific station weighting in the real index (Love and Gannon, 2009), it is expected to reliably reproduce the temporal evolution and relative changes during storms, which is the focus of our study. Furthermore, according to the Biot-Savart Law, the simulated magnetotail contribution to the Dst index  $Dst_{tail}$  is quantified as the z-component of the geomagnetic disturbances generated by the magnetotail currents in the GSM coordinate system (Equation 1).

$$Dst_{tail} = \delta B_z = \frac{1}{4\pi} \sum_{tailgrid} \frac{\mathbf{j} \times \mathbf{R}}{R^3} \Delta V \quad (1)$$

**TABLE 1** Simulated start and end times and corresponding minimum SYM-H index values for all moderate (1–10), intense (11–15), and super geomagnetic storms (16–20) events.

Event number	Start time (UT)	End time (UT)	Min SYM-H (nT)
1	2021-02-28 18:00	2021-03-01 18:00	–80
2	2021-03-19 20:00	2021-03-20 20:00	–60
3	2021-09-17 14:00	2021-09-18 14:00	–73
4	2022-03-05 06:00	2022-03-06 06:00	–60
5	2022-04-10 00:00	2022-04-11 00:00	–67
6	2022-07-01 12:00	2022-07-03 00:00	–67
7	2022-10-14 00:00	2022-10-15 00:00	–78
8	2022-12-07 06:00	2022-12-08 06:00	–68
9	2023-06-15 12:00	2023-06-16 12:00	–84
10	2023-09-12 12:00	2023-09-13 12:00	–84
11	2022-03-13 10:00	2022-03-14 10:00	–114
12	2023-03-23 00:00	2023-03-25 00:00	–170
13	2023-10-21 12:00	2023-10-23 00:00	–108
14	2023-11-25 00:00	2023-11-26 12:00	–109
15	2023-12-01 00:00	2023-12-02 00:00	–136
16	2003-11-19 18:00	2003-11-21 18:00	–490
17	2005-05-15 00:00	2005-05-16 00:00	–305
18	2023-04-23 00:00	2023-04-25 00:00	–233
19	2024-05-10 12:00	2024-05-12 12:00	–518
20	2024-10-10 12:00	2024-10-12 12:00	–390

where  $\mathbf{R}$  is the spatial position of the current density,  $\Delta V$  is the grid volume. The disturbance contributions generated by the grid volumes of all magnetic tail regions are summed up and accumulated to obtain the final magnetic tail Dst index contribution  $Dst_{tail}$ . In this study, the magnetic tail region in the MHD model we selected is:  $-50R_E < x < -5R_E, -10R_E < z < 10R_E$ . There are no restrictions on  $y$ , and these coordinates are all in the GSM coordinate system. This spatial domain was chosen to encompass the main body of the tail current sheet: the  $x$ -range covers the mid-to-distant magnetotail where this current system is dominant, and aims to largely exclude the inner magnetosphere region dominated by the ring current; the  $z$ -range is sufficient to capture the full vertical extent of the current sheet as seen in our simulation results (e.g., Figure 1). The chosen boundaries were informed by the spatial scales considered in prior studies of magnetotail contributions to ground magnetic fields (Turner et al., 2000; Xiao et al., 2016). The potential influence of variations in this spatial definition on our results will be further discussed in Section 5 (Discussion). The temporal resolution of

the index constructed in this study is constrained by the current density  $\mathbf{j}$ , whose determination further depends on the time step of the numerical simulation results. The simulation data employed in this work utilize a 1-min time interval, which aligns with the baseline temporal resolution of the SYM-H index and significantly exceeds the 1-h resolution traditionally adopted in the Dst index. For consistency, the terms “Dst index” and “SYM-H index” hereafter refer interchangeably to this synthesized geomagnetic index with 1-min temporal resolution.

### 3 Simulated events and statistical metrics

The Dst index functions as a fundamental metric for assessing variations in the equatorial geomagnetic field, providing a reliable indicator of magnetospheric current system intensity, with the ring current representing the dominant contributor. As outlined in

Burton et al. (1975) classification framework, geomagnetic storms are divided into four distinct intensity categories based on minimum Dst values: minor storms (−30 to −50 nT), moderate storms (−50 to −100 nT), intense storms (−100 to −200 nT), and super storms (<−200 nT). This study examines a total of 20 geomagnetic storm events, with 18 of them occurring between 2021 and 2024 (see Table 1). All selected events exhibit a clear geomagnetic storm morphology, including a discernible storm sudden commencement (SSC), a well-defined main phase with rapid Dst decrease, and a recovery phase. This ensures our analysis focuses on isolated storm events most suitable for this study. The first ten events (Events 1–10) are categorized as moderate magnetic storms, followed by five intense magnetic storms (Events 11–15), and finally five super storms (Events 16–20). Given the limited number of super storm events observed in recent years, two earlier super storm events were additionally selected to enable a more comprehensive analysis of the relationship between the magnetotail's contribution to the Dst index and storm intensity. Table 1 presents comprehensive event-specific parameters, detailing the simulation temporal boundaries alongside the lowest SYM-H index values observed during each geomagnetic storm. The simulation windows were configured to align with the storm's dynamic evolution: initiations occurred several hours preceding the storm's sudden commencement, while terminations were set once the recovery phase approached stabilization. For all cases, global MHD simulations employed 1-min resolution solar wind measurements (density, velocity, magnetic field orientation, and temperature) extracted from the OMNI database (<https://omniweb.gsfc.nasa.gov/>) at  $x = 30 R_E$  to establish the upstream boundary conditions. Using the solar wind parameters at the model boundary ensures self-consistency and is standard for large-scale, statistical magnetospheric studies (Hu et al., 2007; Ma et al., 2020). While this introduces a fixed timing offset relative to the solar wind arrival at the magnetopause, its impact is negligible for the statistical and trend-based analyses central to this study (e.g., correlation and scaling over storm periods spanning tens of hours). The simulation outputs were produced with identical 1-min temporal resolution to the solar wind input data. The generated Dst indices at this temporal resolution were subsequently compared against the observed SYM-H index derived from the same dataset. During the MHD simulations, a 1-h preheating phase was implemented prior to each storm event, with all simulation data from this period excluded from the subsequent analysis. For instance, in Event 1, solar wind input commenced at 17:00 UT on 28 February 2021, and concluded at 18:00 UT on 1 March 2021. The upstream conditions were initiated precisely 1 hour before the event start time and terminated exactly at the event's conclusion. We provide executable files of the PPMLR-MHD model for simulating each geomagnetic storm event in the studied storm list along with detailed execution instructions, input solar wind and IMF parameters for each event, observed SYM-H indices for validation, and simulation results of the magnetic tail current contribution of the model (Yue et al., 2025).

To accurately determine the contribution of current systems in the magnetotail region from MHD simulations to the Dst index, and to validate the correlation between the Dst index derived from MHD-simulated magnetotail currents and the observed Dst index, two statistical metrics were employed: Prediction Efficiency (PE) and Correlation Coefficient (CC). Prediction Efficiency (PE) quantifies the model's capability in reducing the prediction variance

relative to the observed variance in discrete-time data. It evaluates model effectiveness by comparing the residual prediction variance with the observed variance. The mathematical formulation of PE for discrete-time series (Equation 2) is defined as follows

$$PE = 1 - \frac{\langle (x_{mod} - x_{obs})^2 \rangle}{\sigma_{obs}^2} \quad (2)$$

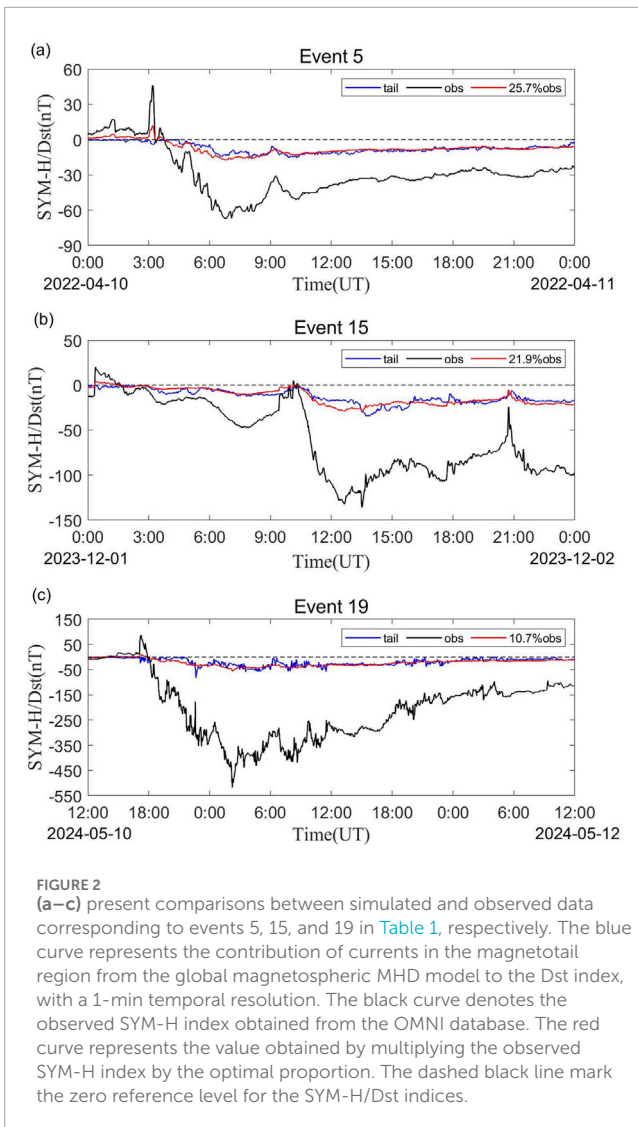
with  $\langle \dots \rangle$  denoting the average value,  $x_{obs}$  representing the measured data points,  $x_{mod}$  indicating the simulated outputs, and  $\sigma_{obs}$  corresponding to the standard deviation (STD) of observations. The averages and standard deviations in the equations are computed using all 1-min data points within the scientifically relevant simulation window for each event (Table 1), i.e., from the simulation start time to end time, excluding the initial 1-h preheating phase. A PE value approaching 1 indicates optimal model performance characterized by nearly perfect agreement between simulated and observed data. A PE value of 0 signifies that the model's performance is equivalent to a scenario where all simulated values equal the observed mean value. Theoretically, PE values can extend to negative infinity, with higher PE values consistently representing closer alignment between simulation results and observational data, thereby reflecting enhanced simulation accuracy.

The Correlation Coefficient (CC) serves as a statistical measure to quantify the degree of linear association between two variables. Its mathematical formulation (Equation 3) is expressed as follows:

$$CC = \frac{\langle (x_{obs} - \bar{x}_{obs})(x_{mod} - \bar{x}_{mod}) \rangle}{\sigma_{obs}\sigma_{mod}} \quad (3)$$

where  $\bar{x}$  is the mean value,  $\sigma_{mod}$  represents the standard deviation of the simulated data. A CC value ranges from −1 to 1, where a value of 1 represents a perfect positive linear correlation and −1 indicates a perfect negative linear correlation. The proximity of CC to 1 signifies a stronger linear relationship between model simulations and observational data. Conversely, CC values approaching zero suggest the absence or negligible presence of a linear association between the two variables. The reason we select both PE and CC as performance metrics is because CC primarily captures the linear correlation between datasets but may not adequately reflect absolute numerical discrepancies. Therefore, PE was incorporated to quantify the absolute differences in magnitude between simulated and observed values.

The procedure to determine the statistically optimal scaling factor (hereafter referred to as the “optimal proportion”) between the simulated magnetotail current proxy and the observed Dst index is as follows. First, the CC between the two time series is calculated. A high CC value indicates a good linear correlation in their temporal evolution. Next, the observed Dst time series is multiplied by a trial scaling factor, and the PE between this scaled series and the simulation is computed. This factor is iteratively adjusted to maximize the PE value. The factor yielding the highest PE is defined as the optimal proportion; it represents the scaling required for the model proxy to best match the observed variation in a statistical sense. It is noted that the CC, which reflects the morphological correlation, remains unchanged regardless of the scaling factor. We emphasize that this optimal proportion is not an exact physical partition of the observed Dst, but rather a robust statistical estimator. It quantifies the scaling factor at which the



temporal evolution of the simulated magnetotail current proxy best matches the observed Dst variation, under the precondition of a strong linear correlation (high CC).

## 4 Simulation results

In this section, we present a comparison between the MHD simulation results and observational data for several geomagnetic storm events listed in Table 1. Figure 2 illustrates the comparison between simulated and observed data for events No. 5, 15, and 19 specified in the table. The blue curve represents contributions from the current in the magnetotail region of the global magnetospheric MHD model to the Dst index, with a 1-min temporal resolution. The black curve denotes the observed SYM-H index obtained from the OMNI database. The red curve indicates values derived by multiplying the observed SYM-H index by the optimal proportion.

Figure 2a presents the moderate geomagnetic storm event on 10 April 2022, corresponding to Event 5 in Table 1. The blue line represents the contribution of magnetotail current to the Dst index

derived from MHD simulations, while the black line shows the observed Dst index with 1-min resolution. Taking this event as an example, we will explain how to determine the proportion of the magnetotail current contribution relative to the Dst index. In this case, the PE value between the blue and black curves is  $-0.807$ , while the CC value is 0.859. Although the significant deviation between the two curves results in a low PE value, the correlation coefficient remains relatively high. Subsequently, we scale the observed Dst index (black line) by different proportions and recalculate the PE value between the scaled curves and the simulated magnetotail current contribution (blue line). The proportion yielding the maximum PE value is defined as the optimal proportion. It should be noted that the CC depends solely on the correlation between the two curves' morphological features, so scaling the black line does not affect the CC value. Our analysis reveals that when the scaling proportion reaches 25.7%, the PE value achieves its maximum of 0.735. Therefore, 25.7% is identified as the optimal proportion. The red line in the figure corresponds to the observed Dst index (black line) multiplied by this optimal proportion.

Figure 2b presents the intense geomagnetic storm event on 1 December 2023, corresponding to Event 15 in Table 1. Following the same methodology as the previous event, the proportion of magnetotail current contribution to the Dst index can be determined. In this case, the PE value between the blue and black curves is  $-0.975$ , while the CC value remains relatively high at 0.868. Through systematic scaling analysis, the optimal proportion is identified as 21.9%, where the PE value reaches its maximum of 0.753. The red line in the figure represents the observed Dst index (black line) scaled by this optimal proportion. Figure 2c displays the super geomagnetic storm event on 10 May 2024, corresponding to Event 19 in Table 1. Applying the identical analytical framework, the proportion of magnetotail current contribution to the Dst index is quantified. The PE value between the blue and black curves initially measures  $-2.034$ , with a CC value of 0.811. The optimization process reveals that scaling the observed Dst index by 10.7% yields the maximum PE value of 0.562, thereby defining 10.7% as the optimal proportion. The red line in this subfigure similarly represents the scaled Dst index using this proportion. Furthermore, a comprehensive analysis of all three subfigures reveals a consistent characteristic: the magnetotail current contributions to the Dst index are predominantly negative and contribute negligibly to the initial phase of the geomagnetic storms.

Table 2 summarizes the magnetotail current contribution proportion to the Dst index and the associated statistical metrics (PE and CC) for all twenty geomagnetic storm events, as derived from a global magnetospheric MHD model. The first ten events (1–10) are moderate storm events, followed by five intense storm events (11–15), and finally five super storm events (16–20). For each event, the table lists the initial and optimal PE, with the optimization process consistently yielding a substantial increase in PE values, confirming the effectiveness of the scaling method. A clear and consistent dependence of the tail current's contribution on storm intensity is revealed. For moderate storms, the tail current contributes a significant and consistent fraction of the total Dst index, with individual event proportions ranging from 23.5% to 25.9% and a group average of 24.8%. As storm intensity increases to the intense category, the average contribution decreases to

TABLE 2 Summary of the magnetotail current contribution proportion and the corresponding statistical metrics (PE and CC) for all storm events.

Event number	Start time (UT)	End time (UT)	Min SYM-H (nT)	Tail contribution proportion	PE_initial	PE_optimal	CC
1	2021-02-28 18:00	2021-03-01 18:00	-80	24.4%	-0.288	0.699	0.838
2	2021-03-19 20:00	2021-03-20 20:00	-60	25.4%	0.150	0.567	0.865
3	2021-09-17 14:00	2021-09-18 14:00	-73	24.2%	-0.660	0.715	0.848
4	2022-03-05 06:00	2022-03-06 06:00	-60	25.9%	-0.917	0.779	0.886
5	2022-04-10 00:00	2022-04-11 00:00	-67	25.7%	-0.807	0.735	0.859
6	2022-07-01 12:00	2022-07-03 00:00	-67	24.7%	0.031	0.711	0.897
7	2022-10-14 00:00	2022-10-15 00:00	-78	25.6%	-0.480	0.675	0.823
8	2022-12-07 06:00	2022-12-08 06:00	-68	25.0%	-1.264	0.704	0.857
9	2023-06-15 12:00	2023-06-16 12:00	-84	23.5%	-0.756	0.673	0.827
10	2023-09-12 12:00	2023-09-13 12:00	-84	23.8%	-1.121	0.727	0.876
1 – 10		Moderate storm	Mean	24.8%			
11	2022-03-13 10:00	2022-03-14 10:00	-114	22.1%	-0.452	0.662	0.822
12	2023-03-23 00:00	2023-03-25 00:00	-170	20.9%	-0.601	0.748	0.875
13	2023-10-21 12:00	2023-10-23 00:00	-108	23.3%	-1.327	0.610	0.805
14	2023-11-25 00:00	2023-11-26 12:00	-109	22.9%	-1.645	0.538	0.817
15	2023-12-01 00:00	2023-12-02 00:00	-136	21.9%	-0.975	0.753	0.868
11 – 15		Intense storm	Mean	22.2%			
16	2003-11-19 18:00	2003-11-21 18:00	-490	10.9%	-0.753	0.688	0.830
17	2005-05-15 00:00	2005-05-16 00:00	-305	17.1%	-0.605	0.766	0.877
18	2023-04-23 00:00	2023-04-25 00:00	-233	18.6%	-1.042	0.634	0.825
19	2024-05-10 12:00	2024-05-12 12:00	-518	10.7%	-2.034	0.562	0.811
20	2024-10-10 12:00	2024-10-12 12:00	-390	13.4%	-1.569	0.660	0.833
16 – 20		Super storm	Mean	14.1%			

22.2%, with values for individual storms falling between 20.9% and 23.3%. This decreasing trend becomes even more pronounced for super storms. Here, the tail current's role diminishes substantially, contributing only 10.7%–18.6% across events, resulting in a group mean of 14.1%. The CC between simulated and observed time series is consistently high across all events, with values predominantly above 0.82, indicating a robust linear relationship in their temporal evolution. These results robustly demonstrate that while the magnetotail current is a major contributor during moderate geomagnetic activity, its relative role in shaping the Dst index becomes progressively less dominant during more extreme events.

## 5 Verification and discussion

### 5.1 Minimum simulated tail current and observed Dst

Table 3 summarizes the minimum values of the simulated magnetotail current contribution ( $Dst_{tail}$ ) for all storm events, along with the corresponding observed SYM-H minima and their ratios. A key result is the systematic increase in the absolute magnitude of the simulated magnetotail current with storm intensity. The  $Dst_{tail}$  minima range from approximately -14 to -22 nT for moderate storms, intensify to between -20 and -34 nT for intense storms,

**TABLE 3** Minimum simulated magnetotail current contribution and its ratio to the observed SYM-H minimum for all storm events (This entire table is newly added in the revised manuscript; its content is not highlighted in red to maintain readability).

Event number	Start time (UT)	End time (UT)	Min SYM-H (nT)	Simulated min $Dst_{tail}$ (nT)	Ratio
1	2021-02-28 18:00	2021-03-01 18:00	-80	-17.2	21.5%
2	2021-03-19 20:00	2021-03-20 20:00	-60	-14.8	24.7%
3	2021-09-17 14:00	2021-09-18 14:00	-73	-15.7	21.5%
4	2022-03-05 06:00	2022-03-06 06:00	-60	-15.6	26.0%
5	2022-04-10 00:00	2022-04-11 00:00	-67	-16.2	24.2%
6	2022-07-01 12:00	2022-07-03 00:00	-67	-15.1	22.5%
7	2022-10-14 00:00	2022-10-15 00:00	-78	-14.2	18.2%
8	2022-12-07 06:00	2022-12-08 06:00	-68	-17.2	25.3%
9	2023-06-15 12:00	2023-06-16 12:00	-84	-21.5	25.6%
10	2023-09-12 12:00	2023-09-13 12:00	-84	-18.6	22.1%
11	2022-03-13 10:00	2022-03-14 10:00	-114	-22.9	20.1%
12	2023-03-23 00:00	2023-03-25 00:00	-170	-32.2	18.9%
13	2023-10-21 12:00	2023-10-23 00:00	-108	-20.3	18.8%
14	2023-11-25 00:00	2023-11-26 12:00	-109	-28.2	25.9%
15	2023-12-01 00:00	2023-12-02 00:00	-136	-34.4	25.3%
16	2003-11-19 18:00	2003-11-21 18:00	-490	-52.1	10.6%
17	2005-05-15 00:00	2005-05-16 00:00	-305	-45.1	14.8%
18	2023-04-23 00:00	2023-04-25 00:00	-233	-39.2	16.8%
19	2024-05-10 12:00	2024-05-12 12:00	-518	-82.5	15.9%
20	2024-10-10 12:00	2024-10-12 12:00	-390	-47.8	12.3%

and further increase to  $-39$  to  $-83$  nT for super storms. This demonstrates a clear physical response of the magnetotail current system to stronger solar wind driving.

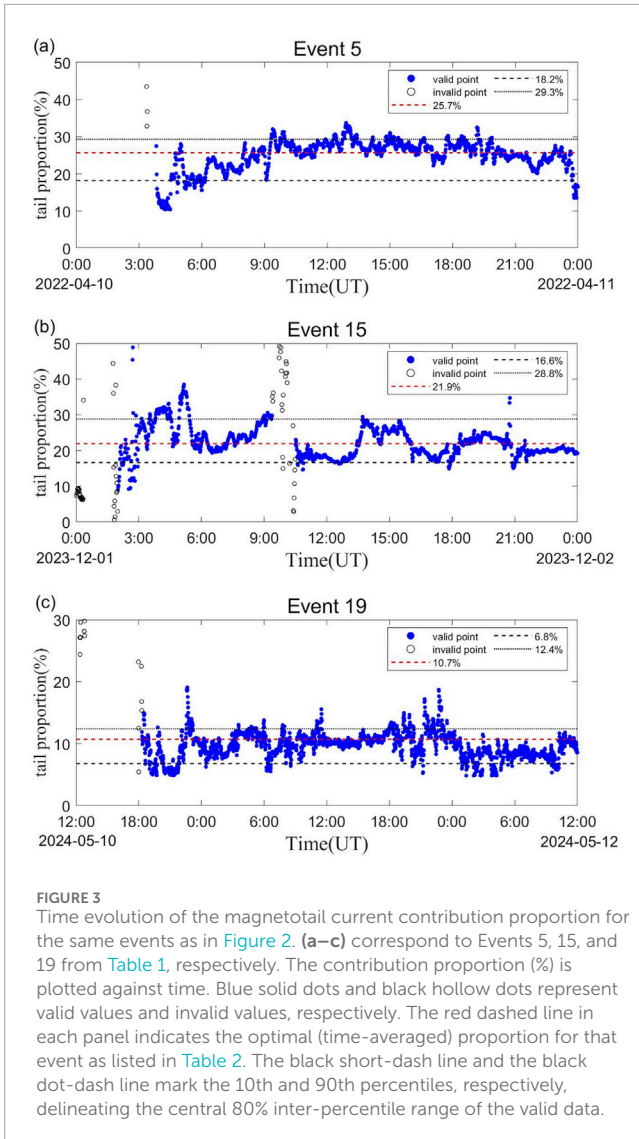
The concurrent analysis of the ratio provides further insight. While the absolute  $Dst_{tail}$  signal strengthens, its relative contribution to the total Dst index shows a decreasing trend (e.g., from 20%–26% for moderate storms to 11%–17% for super storms). This pattern of increasing absolute contribution coupled with a decreasing relative share indicates that other current systems, particularly the ring current, undergo a disproportionately larger enhancement during extreme events. Together, these results quantify the evolving role of the magnetotail current within the magnetospheric current system across different storm intensities.

## 5.2 Temporal variation and error analysis of the contribution

To quantitatively assess the time dependence of the magnetotail current contribution and evaluate the associated uncertainty, we

analyze its high-resolution evolution. Figure 3 presents the minute-by-minute contribution proportion for Events 5 (moderate), 15 (intense), and 19 (super storm), corresponding to the events shown in Figure 2. A meaningful contribution proportion can only be calculated when the observed SYM-H index is negative, as the simulated magnetotail current contribution ( $Dst_{tail}$ ) is invariably negative. Periods with positive SYM-H values, such as during the initial storm sudden commencement or quiet intervals, are excluded from the proportion analysis. In Figure 3, blue solid dots represent valid proportion estimates, while black hollow dots denote invalid periods filtered out by this criterion. The red dashed line in each panel indicates the globally optimal, time-averaged proportion for that event (as listed in Table 2).

Figure 3a presents the moderate geomagnetic storm event on 10 April 2022, corresponding to Event 5 in Table 1. Following the invalid initial phase (before 03:40 UT), the contribution proportion exhibits a coherent temporal structure. It undergoes a gradual increase during the early main phase, displays minor fluctuations around its optimal value of 25.7%, and then experiences a slow



decrease through the recovery phase. To characterize the central range and temporal variability, we calculate the 80% inter-percentile range (IPR) by removing the top and bottom 10% of valid data points. This yields a robust estimate of 18.2%–29.3% for the dominant period of this storm.

Figure 3b presents the intense geomagnetic storm event on 1 December 2023, corresponding to Event 15 in Table 1. This event shows more complex temporal dynamics. After the initial invalid period, an extended interval of moderately negative SYM-H (01:50–09:40 UT) precedes the deep main phase. During this time, the proportion shows significant variability. A second invalid period occurs around 09:40–10:20 UT due to a transient positive SYM-H excursion. The deep main and recovery phases (after 10:20 UT) reveal a clearer pattern similar to Event 5, fluctuating around the optimal 21.9%. A notable outlier spike near 21:00 UT is directly attributable to a sharp, transient spike in the observed SYM-H that was not matched by the simulation. The 80% IPR for all valid data in this event is 16.6%–28.8%.

Figure 3c presents the super geomagnetic storm event on 10 May 2024, corresponding to Event 19 in Table 1. For this extreme

event, the valid analysis period begins around 18:15 UT on May 10. The proportion shows an initial adjustment, stabilizes with minor fluctuations around the optimal 10.7% for an extended duration, and finally decays slowly during recovery. The calculated 80% IPR is 6.8%–12.4%.

The analysis confirms that while the contribution proportion is not constant, its temporal evolution is physically structured and clusters around the globally optimized value for each event. The 80% inter-percentile ranges, derived from the central distribution of valid minute-by-minute estimates, provide a statistically robust measure of the uncertainty arising from time dependence. The detailed temporal analysis presented here for these three representative events illustrates the methodology; the complete set of 80% inter-percentile ranges for all 20 storms will be presented and synthesized in Section 5.4.

### 5.3 Sensitivity to the magnetotail spatial domain

To address the potential impact of defining the magnetotail integration volume on our core results, we conducted a systematic sensitivity analysis. This section evaluates how variations in the spatial boundaries of the magnetotail region influence the derived optimal proportion. The analysis focuses on the three representative events spanning all storm intensity categories: Event 5 (moderate), Event 15 (intense), and Event 19 (super). As mentioned previously, the baseline integration domain is defined as  $-50R_E < x < -5R_E$  and  $|z| < 10R_E$  (unrestricted in  $y$ ). We systematically adjusted each of the three key boundaries— $x_{\max}$  and  $x_{\min}$ , the inner and outer boundaries along the  $x$ -direction, respectively, and  $|z|_{\max}$ , the outer boundary along the  $z$ -direction—to create a suite of alternative domains. For each modified domain and for each of the three storm events, we recalculated the optimal proportion using the procedure outlined in Section 2. The complete results are summarized in Table 4.

The data in Table 4 reveals several informative patterns regarding the sensitivity of our results: Moving the inner boundary  $x_{\max}$  tailward from  $-4R_E$  to  $-6R_E$  and  $-7R_E$ , thereby excluding more of the near-Earth region, results in a monotonic decrease in the optimal proportion for all storm types. This is physically consistent as a smaller integration volume captures less of the tail current. However, moving the boundary earthward to  $-3R_E$  yields a proportion slightly lower than that for  $-4R_E$ , particularly for the intense and super storms. We attribute this non-monotonic behavior to the compression of the dayside magnetosphere during strong storms. An earthward-shifted  $x_{\max} = -3R_E$  boundary will include portions of the magnetopause current system, which contributes a positive ( $\delta B_z > 0$ ) perturbation to Dst, opposite in sign to the magnetotail current. This inclusion partially offsets the negative tail current contribution, leading to a slightly reduced optimal scaling factor.

Variations in the distant tail boundary ( $x_{\min}$  from  $-45R_E$  to  $-55R_E$ ) show no measurable change (within 0.1%) in the optimal proportion compared to the baseline. This indicates that the tail current in the very distant magnetosphere ( $x < -45R_E$ ) contributes negligibly to the ground magnetic perturbation at Earth, and our results are robust to its inclusion or exclusion.

TABLE 4 Sensitivity of the optimal proportion to variations in the magnetotail integration domain for three representative storm events (This entire table is newly added in the revised manuscript; its content is not highlighted in red to maintain readability).

Integration domain definition	Event 5 (moderate)	Event 15 (intense)	Event 19 (super)
Baseline ( $x: [-50, -5]R_E;  z  < 10R_E$ )	25.7%	21.9%	10.7%
<b>Variation of the inner boundary (<math>x_{\max}</math>)</b>			
$x_{\max} = -3R_E$	26.5%	22.2%	10.6%
$x_{\max} = -4R_E$	26.6%	22.4%	10.9%
$x_{\max} = -6R_E$	25.1%	21.4%	10.5%
$x_{\max} = -7R_E$	24.6%	21.1%	10.3%
<b>Variation of the tail length (<math>x_{\min}</math>)</b>			
$x_{\min} = -45R_E$	25.7%	21.9%	10.7%
$x_{\min} = -55R_E$	25.7%	21.9%	10.7%
<b>Variation of the current sheet vertical extent (<math> z _{\max}</math>)</b>			
$ z _{\max} = 8R_E$	24.5%	21.0%	10.4%
$ z _{\max} = 9R_E$	25.3%	21.6%	10.7%
$ z _{\max} = 11R_E$	26.2%	22.2%	10.9%
$ z _{\max} = 12R_E$	26.3%	22.1%	10.8%

Similar to the  $x_{\max}$  variation, reducing the vertical extent ( $|z|_{\max}$  from  $10 R_E$  to  $8$  or  $9 R_E$ ) decreases the proportion, as expected from a smaller integration volume. Expanding it to  $11 R_E$  increases the proportion. Expanding further to  $12 R_E$ , however, shows a divergent response: a continued slight increase for the moderate storm (Event 5) but a slight decrease for the intense and super storms (Events 15 and 19). This pattern is consistent with the physical mechanism described for the  $x_{\max}$  sensitivity. During intense storms, the compression of magnetospheric flank region may cause a widened  $|z|$  domain to encompass more of the magnetopause currents. Their positive contribution counteracts the tail current, explaining the slight reduction in the optimal proportion for the strongest events.

Despite the subtle physical interactions revealed above, the central finding of this sensitivity analysis is the remarkable stability of our core result. Across all tested variations of the integration domain, the optimal proportion for Event 5 consistently remains near 25%, for Event 15 near 22%, and for Event 19 near 11%. The absolute variation for any single event across all tests is confined to a narrow range (e.g., less than  $\pm 2$  percentage points for Event 5). Most importantly, the key ordinal relationship—the systematic decrease in the magnetotail current's optimal scaling factor with increasing storm intensity—remains unequivocally preserved in every single row of Table 4.

Therefore, we conclude that while the precise definition of the magnetotail spatial domain introduces minor quantitative variations, it does not alter the qualitative, storm-intensity-dependent trend that is the principal conclusion of this study.

Our findings are robust to reasonable uncertainties in this methodological choice.

## 5.4 Synthesis and storm-intensity dependence

To synthesize the findings from the preceding sections and present a unified view of the storm-intensity dependence of the magnetotail current contribution, we introduce a comprehensive summary plot (Figure 4). This figure integrates the core results from two distinct methodological approaches for all 20 storm events: (1) the statistically optimal proportion derived from the Prediction Efficiency (PE) optimization (Section 4, represented by solid markers), and (2) the central 80% range of its minute-by-minute temporal evolution (Section 5.2, represented by vertical error bars and shaded regions). The events are visually grouped by storm intensity using light background colors (green for moderate, blue for intense, red for super storms). This synthesized view allows us to robustly assess the storm-intensity dependence of the contribution and its associated uncertainty.

A primary observation is the systematic evolution in the magnitude of temporal variability across storm categories. For moderate storms (Figure 4a), the 80% ranges are consistently wide, typically spanning approximately 10–11 percentage points (e.g., 18.2%–29.3% for Event 1). For super storms (Figure 4b), these ranges contract substantially, often to about 5–8 percentage points (e.g., 6.8%–12.4% for Event 19). This indicates not only a lower

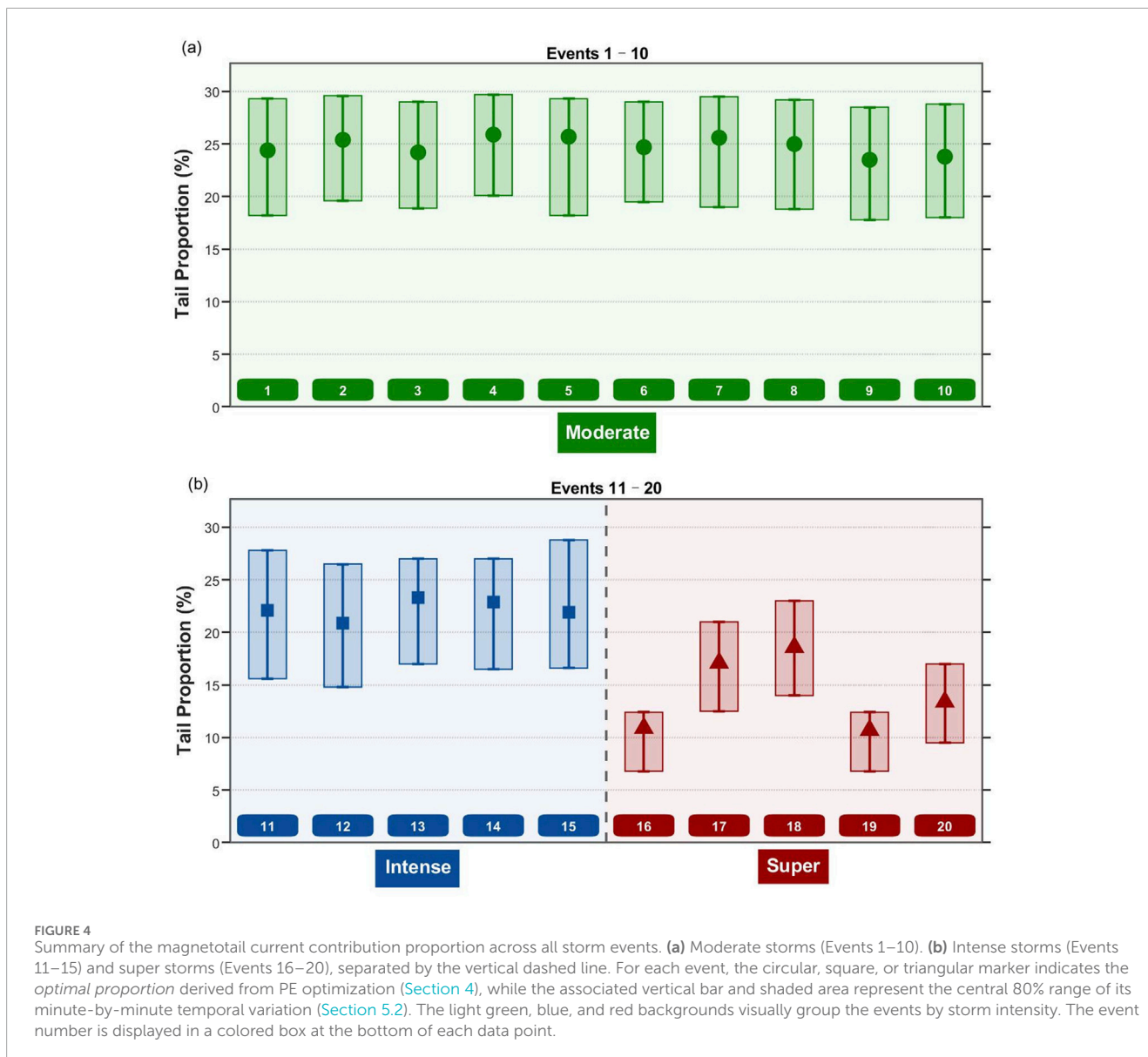


FIGURE 4

Summary of the magnetotail current contribution proportion across all storm events. (a) Moderate storms (Events 1–10). (b) Intense storms (Events 11–15) and super storms (Events 16–20), separated by the vertical dashed line. For each event, the circular, square, or triangular marker indicates the *optimal proportion* derived from PE optimization (Section 4), while the associated vertical bar and shaded area represent the central 80% range of its minute-by-minute temporal variation (Section 5.2). The light green, blue, and red backgrounds visually group the events by storm intensity. The event number is displayed in a colored box at the bottom of each data point.

average contribution but also a reduced temporal scatter during the most extreme events. This visual separation, reinforced by the colored backgrounds, demonstrates that the downward trend in the contribution proportion with increasing storm intensity is robust and exceeds the inherent temporal uncertainty within any single event. The consistent offset between the grouped data, anchored by their respective temporal variation bounds, consolidates the statistical and physical conclusions drawn from the preceding analyses.

To further quantify the dependence of this optimal contribution proportion on storm intensity, we plot it against the minimum SYM-H index for each event in Figure 5. Figure 5 illustrates the relationship between the optimal contribution proportion of magnetotail currents in the MHD model to the Dst index and the minimum SYM-H/Dst values across all geomagnetic storm events.

Simulation results indicate that during moderate geomagnetic storms, the contribution of the magnetotail current to the observed

Dst values typically ranges between 23% and 26%, with an average of 24.8% across ten analyzed moderate storm events. For intense geomagnetic storms, this contribution remains within 20%–24%, averaging 22.2% over five intense storm events. However, during extreme superstorms, the proportion consistently falls below 20%, reaching as low as 10.7% in the exceptionally strong event on 10 May 2024. A linear fitting of all data points in the figure, with the abscissa and ordinate denoted as  $x$  and  $y$  respectively, yields the regression line  $y = 0.033x + 26.931$  (plotted in red). Statistical analysis reveals that the relative contribution of the magnetotail current generally exhibits a decreasing trend with increasing storm intensity, which closely approximates a linear relationship across the studied range. This decrease in relative contribution occurs alongside a systematic increase in the absolute magnitude of the simulated tail current (Section 5.1), confirming that the ring current grows disproportionately during extreme storms.

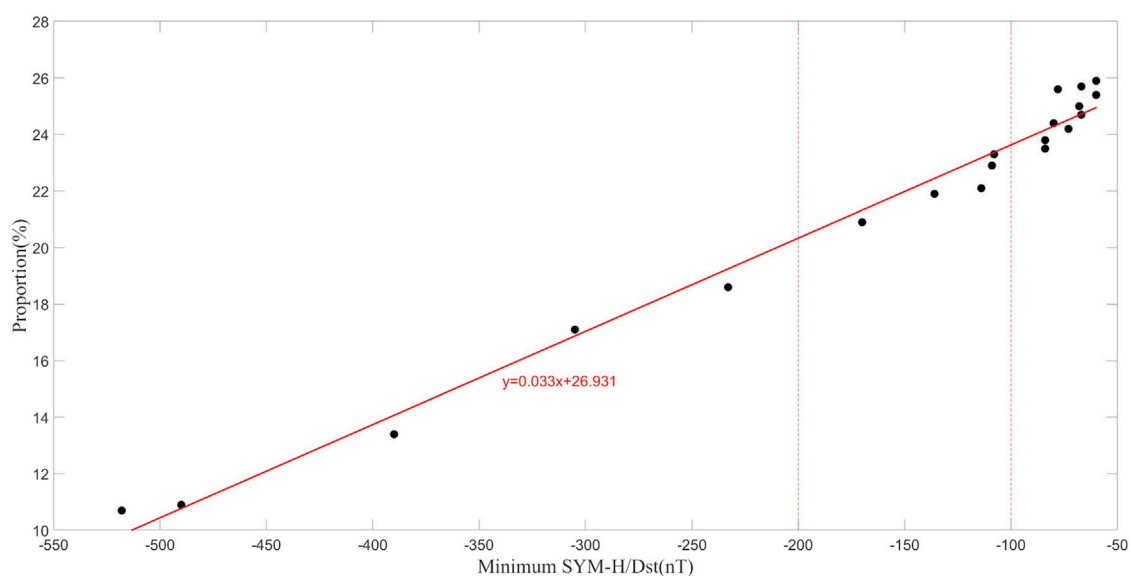


FIGURE 5

The scatter plot shows the relationship between the proportion of MHD model magnetotail current contribution to Dst index and the minimum SYM-H/Dst value in all geomagnetic storm events. Magnetic storms of different intensity types are separated by red dashed lines.

The subsequent analysis compares and discusses the results of this study with those derived from previous literature. Our simulation results, derived from a systematic analysis of twenty geomagnetic storms using a global MHD model, provide a quantitative and storm-intensity-dependent perspective on the long-debated role of magnetotail currents in contributing to the Dst index. The findings robustly confirm and refine several key aspects previously suggested in the literature. The average contribution of 24.8% during moderate storms aligns remarkably well with the early estimates of approximately one-quarter by [Turner et al. \(2000\)](#) and the 20%–25% range reported by [Ohtani et al. \(2001\)](#). This consistency across different methodologies, including empirical modeling, statistical studies, and now global MHD simulations, strengthens the consensus that the tail current is a significant, non-negligible component of the Dst index during moderate geomagnetic activity. Furthermore, the decreasing trend in the relative contribution of the tail current observed in this study—with values declining from 24.8% during moderate storms to 22.2% during intense storms and further dropping to 14.1% during superstorms—supports some of the conclusions of [Kalegaev et al. \(2005\)](#) and [Kalegaev and Makarenkov \(2008\)](#). These authors proposed that the ring current becomes increasingly dominant with storm intensification, while the tail current effect approaches saturation. Consistent with this view, our quantitative results show that the relative share of the magnetotail current diminishes with storm intensification. The derived linear relationship  $y = 0.033x + 26.931$  provides a simplified empirical scaling relation between the statistically optimized tail current proxy and storm intensity. Our MHD simulation results, which show a significant contribution of the magnetotail current to the Dst index during the storm main phase, are consistent with the perspective presented by [Pulkkinen et al. \(2022\)](#). Our study, by spanning a wide range of storm intensities with a consistent methodology, bridges the

gaps between previous event-specific or model-specific conclusions. It validates the general picture that while the magnetotail current is a robust and major contributor during moderate disturbances, its relative importance is superseded by the intensifying ring current as geomagnetic activity escalates to super storm levels. Since the MHD model employed in this study does not incorporate a coupled inner magnetospheric model, it is incapable of accurately resolving the ring current dynamics. Consequently, this study focuses exclusively on the tail current systems within the magnetotail region. The potential modifications to the magnetotail current structure arising from the integration of inner magnetospheric coupling and ring current physics into the MHD framework will be systematically investigated in our future research endeavors.

## 6 Summary

This study utilized a global magnetospheric MHD model to compute the contribution of magnetotail currents to geomagnetic disturbances by integrating the simulated current density, yielding a magnetic perturbation at Earth center as a Dst-like proxy. The optimal proportion of this contribution relative to the observed SYM-H index was determined through a statistical scaling procedure for each event. To our knowledge, this represents the first systematic quantification of this contribution across a wide range of storm intensities using a physics-based global model. The simulation results across twenty geomagnetic storms reveal a clear storm-intensity dependence in the role of the magnetotail current. During moderate storms, its statistically optimized contribution to the SYM-H index typically ranges between 23% and 26%, with a group average of 24.8%. For intense storms, the contribution ranges between 20% and 24%, with a group average of 22.2%. In super storms, the proportion falls consistently below 20%, averaging 14.1%, with

values as low as 10.7%. Two key findings underpin this trend. First, the absolute magnitude of the simulated magnetotail current signal itself increases systematically with storm intensity. Second, the temporal evolution of the instantaneous contribution proportion is physically structured and clusters stably around the optimal value for each event. Consequently, the decreasing relative contribution with increasing storm intensity is a robust statistical and physical result. It indicates that the total geomagnetic disturbance grows at a rate that significantly outpaces the strengthening of the magnetotail current during extreme events. In summary, this study provides quantitative, model-based evidence that the magnetotail current is a significant and consistent contributor during moderate to intense geomagnetic storms, but its relative share in the overall disturbance diminishes substantially during the most extreme superstorms.

## Data availability statement

Solar wind and interplanetary magnetic field (IMF) parameters, along with 1-minute resolution SYM-H index data, are publicly accessible via the OMNI database ([https://omniweb.gsfc.nasa.gov/form/omni\\_min.html](https://omniweb.gsfc.nasa.gov/form/omni_min.html)). We provide executable files of the PPMLR-MHD model for simulating each geomagnetic storm event in the studied storm list along with detailed execution instructions, input solar wind and IMF parameters for each event, observed SYM-H indices for validation, and simulation results of the magnetic tail current contribution of the model (Yue et al., 2025).

## Author contributions

JY: Conceptualization, Data curation, Formal Analysis, Investigation, Methodology, Project administration, Software, Validation, Visualization, Writing – original draft, Writing – review and editing. XG: Conceptualization, Formal Analysis, Funding acquisition, Investigation, Methodology, Project administration, Resources, Software, Supervision, Writing – original draft, Writing – review and editing. YW: Investigation, Software, Writing – review and editing. CW: Funding acquisition, Project administration, Resources, Supervision, Writing – review and editing.

## Funding

The author(s) declared that financial support was received for this work and/or its publication. This research was supported

## References

- Artemyev, A., and Zelenyi, L. (2013). Kinetic structure of current sheets in the earth magnetotail. *Space Sci. Rev.* 178, 419–440. doi:10.1007/s11214-012-9954-5
- Artemyev, A., Lu, S., El-Alaoui, M., Lin, Y., Angelopoulos, V., Zhang, X., et al. (2021). Configuration of the earth's magnetotail current sheet. *Geophys. Res. Lett.* 48. doi:10.1029/2020gl092153
- Asikainen, T., Maliniemi, V., and Mursula, K. (2010). Modeling the contributions of ring, tail, and magnetopause currents to the corrected dst index. *J. Geophys. Res.* 115. doi:10.1029/2010ja015774

by the National Natural Science Foundation of China (Grants 42188105, 42150101 and 42304189), the Macau Science and Technology Development Fund (Grant FDCT-25-055-SSI), the National Key R&D Program of China (Grant 2021YFA0718600), and the “PanDeng” Program of the National Space Science Center, Chinese Academy of Sciences.

## Acknowledgements

We acknowledge the provision of data resources from the Space Physics Data Facility at NASA Goddard Space Flight Center (GSFC), specifically through the OMNIWeb service and the OMNI dataset. The Dst index, SYM-H index, and solar wind data employed in this research are publicly accessible via the NASA National Space Science Data Center (NSSDC) at <https://nssdc.gsfc.nasa.gov/>.

## Conflict of interest

The author(s) declared that this work was conducted in the absence of any commercial or financial relationships that could be construed as a potential conflict of interest.

## Generative AI statement

The author(s) declared that generative AI was not used in the creation of this manuscript.

Any alternative text (alt text) provided alongside figures in this article has been generated by Frontiers with the support of artificial intelligence and reasonable efforts have been made to ensure accuracy, including review by the authors wherever possible. If you identify any issues, please contact us.

## Publisher's note

All claims expressed in this article are solely those of the authors and do not necessarily represent those of their affiliated organizations, or those of the publisher, the editors and the reviewers. Any product that may be evaluated in this article, or claim that may be made by its manufacturer, is not guaranteed or endorsed by the publisher.

- Bame, S., Asbridge, J., Felthouser, H., Hones, E. W., and Strong, I. (1967). Characteristics of the plasma sheet in the earth's magnetotail. *J. Geophys. Res.* 72, 113–129. doi:10.1029/jz072i001p00113
- Bird, M. (1974). Solar wind access to the plasma sheet along the flanks of the magnetotail. *Planet. Space Sci.* 23, 27–40. doi:10.1016/0032-0633(75)90065-3
- Burton, R. K., McPherron, R. L., and Russell, C. T. (1975). An empirical relationship between interplanetary conditions and dst. *J. Geophys. Res.* (1896-1977) 80, 4204–4214. doi:10.1029/JA080i031p04204

- Chen, Y., Tóth, G., Cassak, P., Jia, X., Gombosi, T., Slavin, J., et al. (2017). Global three-dimensional simulation of earth's dayside reconnection using a two-way coupled magnetohydrodynamics with embedded particle-in-cell model: initial results. *J. Geophys. Res. Space Phys.* 122, 10,318–10,335. doi:10.1002/2017ja024186
- Frank, L. (1985). Plasmas in the earth's magnetotail. *Space Sci. Rev.* 42, 211–240. doi:10.1007/bf00218233
- Frank, L., McPherron, R., Decoster, R., Burek, B. G., Ackerson, K., and Russell, C. (1981). Field-aligned currents in the earth's magnetotail. *J. Geophys. Res.* 86, 687–700. doi:10.1029/ja086ia02p00687
- Ganushkina, N., Pulkkinen, T., Kubyskhina, M., Singer, H., and Russell, C. (2004). Long-term evolution of magnetospheric current systems during storms. *Ann. Geophys.* 22, 1317–1334. doi:10.5194/angeo-22-1317-2004
- Ganushkina, N., Liemohn, M., Kubyskhina, M., Ilie, R., and Singer, H. (2010). Distortions of the magnetic field by storm-time current systems in earth's magnetosphere. *Ann. Geophys.* 28, 123–140. doi:10.5194/angeo-28-123-2010
- Ganushkina, N., Dubyagin, S., Kubyskhina, M., Liemohn, M., and Runov, A. (2012). Inner magnetosphere currents during the cir/hss storm on July 21–23, 2009. *J. Geophys. Res.* 117. doi:10.1029/2011ja017393
- Guo, X. (2015). An extended hllc riemann solver for the magneto-hydrodynamics including strong internal magnetic field. *J. Comput. Phys.* 290, 352–363. doi:10.1016/j.jcp.2015.02.048
- Guo, X., Florinski, V., and Wang, C. (2016). The hlld riemann solver based on magnetic field decomposition method for the numerical simulation of magneto-hydrodynamics. *J. Comput. Phys.* 327, 543–552. doi:10.1016/j.jcp.2016.09.057
- Hesse, M., and Cassak, P. (2020). Magnetic reconnection in the space sciences: past, present, and future. *J. Geophys. Res. Space Phys.* 125, e2018JA025935. doi:10.1029/2018ja025935
- Hu, Y., Guo, X., and Wang, C. (2007). On the ionospheric and reconnection potentials of the earth: results from global mhd simulations. *J. Geophys. Res.* 112. doi:10.1029/2006ja012145
- Iyemori, T. (1990). Storm-time magnetospheric currents inferred from mid-latitude geomagnetic field variations. *J. Geomagnetism Geoelectricity* 42, 1249–1265. doi:10.5636/jgg.42.1249
- Ji, H., Daughton, W., Jara-almonte, J., Le, A., Stanier, A., and Yoo, J. (2022). Magnetic reconnection in the era of exascale computing and multiscale experiments. *Nat. Rev. Phys.* 4, 263–282. doi:10.1038/s42254-021-00419-x
- Kalegaev, V., and Ganushkina, N. (2013). Global magnetospheric dynamics during magnetic storms of different intensities. *Geophys. Monograph* 155, 293–300. doi:10.1029/155gm31
- Kalegaev, V., and Makarenkov, E. V. (2008). Relative importance of ring and tail currents to dst under extremely disturbed conditions. *J. Atmos. Solar-Terrestrial Phys.* 70, 519–525. doi:10.1016/j.jastp.2007.08.029
- Kalegaev, V., Ganushkina, N., Pulkkinen, T., Kubyskhina, M., Singer, H., and Russell, C. (2005). Relation between the ring current and the tail current during magnetic storms. *Ann. Geophys.* 23, 523–533. doi:10.5194/angeo-23-523-2005
- Kamide, Y. (1982). The relationship between field-aligned currents and the auroral electrojets: a review. *Space Sci. Rev.* 31, 127–243. doi:10.1007/bf00215281
- Liemohn, M., Ganushkina, N., Zeeuw, D. D. D., Rastatter, L., Kuznetsova, M., Welling, D., et al. (2018). Real-time swmf at ccmc: assessing the dst output from continuous operational simulations. *Space weather*. 16, 1583–1603. doi:10.1029/2018SW001953
- Liu, J., Angelopoulos, V., Runov, A., and Zhou, X. (2013). On the current sheets surrounding dipolarizing flux bundles in the magnetotail: the case for wedgelets. *J. Geophys. Res. Space Phys.* 118, 2000–2020. doi:10.1002/jgra.50092
- Love, J., and Gannon, J. (2009). Revised dst and the epicycles of magnetic disturbance: 1958–2007. *Ann. Geophys.* 27, 3101–3131. doi:10.5194/angeo-27-3101-2009
- Ma, X., Nykyri, K., Dimmock, A., and Chu, C. (2020). Statistical study of solar wind, magnetosheath, and magnetotail plasma and field properties: 12+ years of themis observations and mhd simulations. *J. Geophys. Res. Space Phys.* 125, e2020JA028209. doi:10.1029/2020ja028209
- Nakamura, R. (2007). Substorms and their solar wind causes. *Space Sci. Rev.* 124, 91–101. doi:10.1007/s11214-006-9131-9
- Nishida, A. (2000). The earth's dynamic magnetotail. *Space Sci. Rev.* 91, 507–577. doi:10.1023/a:1005223124330
- Ohtani, S., Nosé, M., Rostoker, G., Singer, H., Lui, A., and Nakamura, M. (2001). Storm-substorm relationship: contribution of the tail current to. *J. Geophys. Res.* doi:10.1029/2000ja000400
- Patra, S., Spencer, E., Horton, W., and Sojka, J. (2011). Study of dst/ring current recovery times using the windmi model. *J. Geophys. Res.* 116. doi:10.1029/2010ja015824
- Pulkkinen, T., Brenner, A., Shidi, Q. A., and Tóth, G. (2022). Statistics of geomagnetic storms: global simulations perspective. *Front. Astronomy Space Sci.* 9. doi:10.3389/fspas.2022.972150
- Rastätter, L., Kuznetsova, M. M., Glocher, A., Welling, D., Meng, X., Raeder, J., et al. (2013). Geospace environment modeling 2008–2009 challenge: dst index. *Space weather*. 11, 187–205. doi:10.1002/swe.20036
- Ridley, A. J., Gombosi, T. I., Sokolov, I. V., Tóth, G., and Welling, D. T. (2010). Numerical considerations in simulating the global magnetosphere. *Ann. Geophys.* 28, 1589–1614. doi:10.5194/angeo-28-1589-2010
- Rostoker, G. (1996). Phenomenology and physics of magnetospheric substorms. *J. Geophys. Res. Space Phys.* 101, 12955–12973. doi:10.1029/96ja00127
- Rostoker, G., Akasofu, S., Baumjohann, W., Kamide, Y., and McPherron, R. (1988). The roles of direct input of energy from the solar wind and unloading of stored magnetotail energy in driving magnetospheric substorms. *Space Sci. Rev.* 46, 93–111. doi:10.1007/bf00173876
- Runov, A., Angelopoulos, V., Artemyev, A., Weygand, J., Lu, S., Lin, Y., et al. (2021). Global and local processes of thin current sheet formation during substorm growth phase. *J. Atmos. Solar-Terrestrial Phys.* 220, 105671. doi:10.1016/j.jastp.2021.105671
- Skoug, R., Thomsen, M., Henderson, M., Funsten, H., Reeves, G., Pollock, C., et al. (2003). Tail-dominated storm main phase: 31 march 2001. *J. Geophys. Res.* 108, 1259. doi:10.1029/2002ja009705
- Sugiura, M. (1960). The average morphology of geomagnetic storm with sudden commencement. *Abhandl. Akad. Wiss. Gottingen. Math-Physik. Kl. Sonderh.* 4, 53.
- Temerin, M., and Li, X. (2006). Dst model for 1995–2002. *J. Geophys. Res.* 111. doi:10.1029/2005ja011257
- Torbert, R., Burch, J., Phan, T., Hesse, M., Argall, M., Shuster, J., et al. (2018). Electron-scale dynamics of the diffusion region during symmetric magnetic reconnection in space. *Science* 362, 1391–1395. doi:10.1126/science.aat2998
- Tsyganenko, N. (2002). A model of the near magnetosphere with a dawn-dusk asymmetry 2. parameterization and fitting to observations: a new magnetosphere magnetic field model, 2. *J. Geophys. Res.* 107. doi:10.1029/2001ja000220
- Turner, N. E., Baker, D. N., Pulkkinen, T. I., and McPherron, R. L. (2000). Evaluation of the tail current contribution to dst. *J. Geophys. Res. Space Phys.* 105, 5431–5439. doi:10.1029/1999JA000248
- Wanliss, J. A., and Showalter, K. M. (2006). High-resolution global storm index: dst versus sym-h. *J. Geophys. Res.* 111. doi:10.1029/2005ja011034
- Xiao, S., Zhang, T., Ge, Y., Wang, G., Baumjohann, W., and Nakamura, R. (2016). A statistical study on the shape and position of the magnetotail neutral sheet. *Ann. Geophys.* 34, 303–311. doi:10.5194/angeo-34-303-2016
- Yue, J., Guo, X., Wang, Y., and Wang, C. (2025). Dataset for contribution of magnetotail currents to dst index during different intensity magnetic storms: a global MHD. *Model Study*. doi:10.57760/sciencedb.space.03358